REGULAR ARTICLE

blood advances

Bone marrow transplantation prevents right ventricle disease in the *caveolin-1*–deficient mouse model of pulmonary hypertension

Kewal Asosingh,[1] Nicholas Wanner,[1] Kelly Weiss,[1] Kimberly Queisser,[1] Liya Gebreab,[2] Biruk Kassa,[2] Eric Stuehr,[1] Brian Graham,[2] and Serpil Erzurum[1,3]

[1]Department of Pathobiology, Lerner Research Institute, The Cleveland Clinic, Cleveland, OH; [2]Department of Medicine, University of Colorado Anschutz Medical Campus, Denver, CO; and [3]Department of Pathobiology, Respiratory Institute, The Cleveland Clinic, Cleveland, OH

Key Points

- *Caveolin-1* deficiency in hematopoietic stem cells induces right heart disease.
- Healthy BM protects the right heart from maladaptation.

Accumulating evidence shows a causative role for the bone marrow (BM) in the genesis and progression of pulmonary hypertension (PH). Engraftment of BM hematopoietic stem cells from PH patients to mice reproduces the cardiopulmonary pathology of PH. However, it is unknown whether healthy BM can prevent the development of right heart disease. *Caveolin-1*–deficient (*CAV-1* KO) mice develop cardiopulmonary disease with manifestations resembling PH, including elevated right ventricular (RV) systolic pressure (RVSP), RV hypertrophy, and pulmonary endothelial proliferative disease. Here, we hypothesize that engraftment of healthy BM to *CAV-1* KO mice will prevent pulmonary vascular remodeling and development of the cardiopulmonary disease. *CAV-1* KO mice and wild-type (WT) mice underwent transplantation with WT or *CAV-1* KO BM. Hematopoietic differentiation was analyzed by flow cytometry. Pulmonary endothelial remodeling was quantified by CD31 image analysis. RVSP and RV cardiomyocyte area or Fulton's index were used to analyze RV hypertrophy. Maladaptive RV hypertrophy was determined by quantification of RV fibrosis. Transplantation of *CAV-1* KO BM into healthy recipient WT mice led to elevation of RVSP, RV hypertrophy, and pulmonary endothelial remodeling. Reconstitution of *CAV-1* KO with WT BM prevented spontaneous development of PH, including elevation of RVSP and maladaptive RV hypertrophy, but not pulmonary endothelial remodeling. Healthy BM has a protective role in the right ventricle independent of pulmonary vascular disease.

Introduction

Pulmonary hypertension (PH) is a heterogeneous group of diseases characterized by severe remodeling of the pulmonary artery wall, increased right ventricular (RV) systolic pressure (RVSP), RV hypertrophy, and failure.[1]

Caveolin-1 (CAV-1) is the main protein in organelles called caveolae.[2,3] These plasma membrane invaginations play critical roles in many processes, including cell signaling,[4-6] transport,[7,8] cell cycle regulation,[9-11] and mechanosensing.[12] CAV-1 is expressed by structural cells, including endothelial cells, adipocytes, fibrocytes, and type I pneumocytes, and is induced during adipocyte differentiation.[13,14] CAV-1 is constitutively expressed in the bone marrow (BM).[15-17] Several reports show that CAV-1 is involved in human PH. Expression of CAV-1 in patient pulmonary arterial endothelial cells is decreased in pulmonary arterial hypertension (PAH).[18-20] In pulmonary arterial endothelial cells, CAV-1 regulates BMPR2 signaling, which is a major dysfunctional pathway in familial and idiopathic forms of PH.[21] *CAV-1* mutation has been reported in a familial form of PH.[22] BM hematopoietic stem cells (HSCs) from patients with a *CAV-1* mutation that were engrafted in nonobese diabetic severe combined immunodeficiency mice led to severe

Submitted 2 November 2016; accepted 22 February 2017. DOI 10.1182/bloodadvances.2016002691.

pulmonary vascular remodeling and RV hypertrophy.[23] Data from other animal models further support the essential role for CAV-1 in PH. Monocrotaline-induced PH in rats is associated with disruption of endothelial CAV-1 rafts, and restoration of CAV-1 function in this model inhibited the development of PH and RV hypertrophy.[24,25] *CAV-1*–deficient (*CAV-1* KO) mice have increased pulmonary microcapillary proliferation and spontaneously develop increased RV systolic pressure (RVSP), RV hypertrophy, and fibrosis as they age over time.[26,27] The development of PH in *CAV-1* KO mice is accelerated by exposing animals to hypoxia.[28]

We and others have reported a myeloid/BM origin of PH. Engraftment of serotonin 2B receptor–deficient BM in wild-type (WT) mice protected against the development of hypoxia-induced pulmonary vascular remodeling and elevation of RVSP in mice.[29] Unfortunately, RV hypertrophy was not evaluated in this study. In a *Bmpr2* mutant model that spontaneously developed PH without right ventricular remodeling, pulmonary vascular remodeling and elevation of RVSP were dependent on the BM.[30] Xenotransplantation of PH patient BM HSCs into nonobese diabetic severe combined immunodeficiency mice induced pulmonary angiogenic remodeling and RV hypertrophy.[23] Moreover, HSCs in the BM of PH patients were skewed in the myeloid differentiation toward megakaryocyte-erythroid lineage.[23] Pulmonary vascular disease and RV remodeling are key characteristics of PH, but the connection between these 2 processes and whether or not healthy BM can inhibit maladaptation of the right heart have not been addressed.

Here, we tested the hypothesis whether transplantation of healthy BM can attenuate pulmonary vascular remodeling and right heart disease using the *CAV-1* KO mouse as a model system. The results show that *CAV-1* KO mice have abnormal myelopoiesis similar to human PH. BM from *CAV-1* KO mice transfers the PH phenotype to healthy mice. Reconstitution of *CAV-1* KO BM with healthy BM blunts the spontaneous development of PH, including normalization of RVSP, inhibition of RV hypertrophy, and right heart fibrosis, but it does not decrease pulmonary vascular remodeling.

Methods

Animals

CAV-1 KO mice on the C57BL6 background were purchased from JAX Mice (The Jackson Laboratory, Bar Harbor, ME) and bred in-house. Male or female KO or WT mice were used for all experiments.

In some experiments, animals were exposed to hypoxia (10% oxygen) for 3 weeks. A chamber fitted with passive ventilation ports (Small Chamber 38 cm × 51 cm × 51 cm; BioSpherix, Redfield, NY) and attached to a secured liquid nitrogen tank to regulate the level of oxygen inside the chamber was used for hypoxia experiments. The atmospheric condition inside the chamber was set at normal atmospheric pressure with 10% oxygen that was maintained by a highly efficient oxygen sensor (ProOx model 360, BioSpherix). The oxygen sensor was calibrated according to the manufacturer's instruction. To control the level of oxygen in the hypoxia chamber, a single set point of 10% oxygen with alarm at 11% was applied.

BM transplantations were performed at the age of 4 weeks. Animals undergoing BM transplantation received a sublethal dose of whole-body irradiation (total irradiation dose of 1000 cGy) to deplete the BM before intravenous injection of 2.5 to 5 × 10^6 BM mononuclear cells from donor mice.

RVSP was measured at end points. For this purpose anesthetized mice (pentobarbital 80 mg/kg body weight) were placed on a heating pad in the supine position and secured by placing tape over the extremities. A suture string around the front incisors was used to pull the head down. The skin overlying the trachea was cut followed by dissection of remaining tissue around the trachea. The trachea was nicked with fine curved scissors and a small metal tracheostomy tube connected to a mouse ventilator (Harvard Apparatus) was inserted into the airway. Ventilator settings were 150 μL/stroke at 200 strokes/min. The chest cavity was subsequently opened by a longitudinal incision through the center of the sternum. Metal retractors were used to secure the opening. Max Details Spectacles (Fine Science Tools, Foster City, CA) was used to gently insert the tip of a 25G needle through the RV wall. The needle was then removed, and an SPR-1000 Mikro-Tip Catheter (Millar, Houston, TX) was threaded into the right ventricle. RV pressure and heart rate were recorded using a Millar Pressure Control Unit. Cervical dislocation was performed after this procedure to kill the mouse. The heart was removed followed by dissection of the free RV wall. The Fulton index [right/(left + septum) ventricular weight] was calculated as a measure of RV hypertrophy.[31]

All animal procedures were approved by the Cleveland Clinic Institutional Animal Care and Use Committee.

Cardiac myocyte stereologic and planimetric analysis

Formalin-fixed and paraffin-embedded histologic sections of mouse RV tissue were stained with fluorescein-labeled wheat germ agglutinin to identify myocyte cell membranes (Vector, 1:500) and 4′-6-diaminidino-2-phenylindole overnight at 4°C. The identity of the slides was masked. A total of 12 to 15 images at ×40 magnification were randomly captured of each sample. The green channel of each image was thresholded using Metamorph (v6.3; MDS Analytical Technologies, Sunnyvale, CA) to demarcate myocytes. Planimetric analysis of myocyte cross-sectional area was performed by determining the cross-sectional area of all myocytes within the image, requiring the length-to-breadth ratio for each be ≤2 to ensure that transverse cross-sections are close to a circular profile.

Flow cytometry

BM cells were isolated from the front and hind leg bones and strained through a 40-μm cell strainer. Red blood cells were lysed using ammonium chloride, and BM cells were frozen at −80°C in fetal bovine serum containing 10% dimethyl sulfoxide for batch analysis. For immunophenotyping, cells were thawed in a 10-fold volume of PBS before staining with a live/dead dye. To block nonspecific binding, cells were preincubated in 2% normal goat serum before adding antibodies (see Table 1 for more information). Streptavidin Alexa Fluor 700 was used as a secondary reagent to detect lineage-biotin. Samples were analyzed using the LSRFortessa (BD Biosciences) equipped with five lasers (355 nm, 407 nm, 488 nm, 561 nm, and 641 nm). SPHERO Ultra Rainbow Calibration Kit (Spherotech, Lake Forest, IL) was used to standardize the fluorescence channels for day-to-day variation. AbC total antibody compensation bead kit (Life Technologies) was used to perform single color compensation, while cells were used for live/dead dye compensation. In addition to the fully stained samples, unstained and fluorescence minus one (FMO) samples were prepared with 500 000 events being collected for FMO tubes and at least 750 000 events collected for full panel stained tubes. All data were saved as list mode files and analyzed using FlowJo V.10.1 software (Tree Star, Ashland, OR).

Trichrome staining and quantification

Trichrome staining was used to visualize and measure RV fibrosis[28,32,33] A Leica SCN400 F slide scanner (Leica Microsystems, Wetzlar, Germany) was used to scan images of whole slides at ×20 magnification. Image Pro Plus 7.0. software was use for quantification of fibrosis area/total tissue area. Thresholding criteria were set for fibrosis stained blue by trichrome (collagen deposition) using test images. Identical selection criteria were applied to all images.

CD31 immunohistochemistry and quantification of CD31 area

Paraffin-embedded formalin-fixed mouse lung tissue was sectioned at 5 μm. Immunohistochemistry staining was performed using the Discovery ULTRA automated stainer from Ventana Medical System (Tuscon, AZ). In brief, antigen retrieval was performed using a citrate-based buffer (Discovery RiboCC, 790-107; Ventana), pH 6.0, for 32 minutes at 91°C. Slides were

Table 1. Antibodies and stains used for flow cytometry

Antibody or probe	Vendor	Dilution	Laser (nm)	Dichroic	Filter (nm)
Sca1 APC	eBioscience	1/200	641	–	670/30
c-Kit FITC	BD Biosciences	1/50	488	505LP	515/20
CD34 eFluor 450	eBioscience	1/50	407	–	450/50
CD16/CD32 PE	eBioscience	1/200	561	–	582/15
CD135 PE	eBioscience	1/50	561	–	582/15
Lineage cocktail-biotin					
CD11b	BD Biosciences	1/100	N/A	N/A	N/A
CD8as	BD Biosciences	1/200	N/A	N/A	N/A
TER-119	BD Biosciences	1/400	N/A	N/A	N/A
CD4	BD Biosciences	1/400	N/A	N/A	N/A
CD45R	BD Biosciences	1/400	N/A	N/A	N/A
Ly-6G + Ly-6C	BD Biosciences	1/25	N/A	N/A	N/A
Streptavidin Alexa Fluor 700	Life Technologies	1/25	641	685LP	730/45
Live/dead blue stain	Life Technologies	1/1000	355	–	450/50

APC, allophycocyanin; FITC, fluorescein isothiocyanate; N/A, not applicable.

incubated with rabbit anti–mouse CD31 (Santa Cruz Biotechnology, Dallas TX), at a 1:50 dilution, for 1 hour at 37°C. The antibody was visualized using the OmniMap anti–rabbit horseradish peroxidase secondary (760-4311; Ventana) and the ChromoMap 3,3′-diaminobenzidine (DAB) detection kit (760-159; Ventana). Lastly, the slides were counterstained with hematoxylin and bluing. A Leica SCN400 F slide scanner (Leica Microsystems) was used to scan images of whole slides at ×20 magnification. Tiff files (1:1) were extracted from these scans for analysis using SCN-viewer software (written in-house for the Imaging Core). Analysis performed by the DAB Stain Analysis IQbot is fully automated and requires no interaction by an observer to generate output metrics and images. Briefly, for an input image consisting of a histological tissue cross-section stained with DAB (brown-orange hue) and counterstained with hematoxylin (blue hue), the IQbot performs a k-means analysis to segment the tissue area present (tissue mask). Summing pixels in this mask provides the total tissue area. Subsequently, the original input image is smoothed using a low-pass filter and a color-cube–based DAB profile is applied to brown segment signal within the image (DAB mask). Any segmented regions <5 pixels are removed from the DAB mask and a dilated version of the tissue mask is subtracted to remove non–tissue-related, nonspecific staining. The purpose of the tissue mask dilation before subtraction is to remove the contribution of chromatic aberrations often present at the edges of tissue. Summing pixels in the final DAB mask and counting regions of DAB staining provide total positive nuclei/region area and positive nuclei/region counts, respectively. Finally, segmented DAB regions are pseudocolored green and superimposed upon the original image to enable visual confirmation of the algorithm's ability to segment DAB, and the binary tissue mask is saved to confirm that the tissue present in the image is also segmented appropriately.

Statistical analysis

Statistical analysis was performed using JMP 5.1 software program. Analysis of variance (ANOVA) was used for comparison of mean values across groups. P values $< .05$ were considered as significant. Student t-test was used for comparison of 2 means followed by Bonferroni correction for multiple comparisons.

Results

Skewed myeloid differentiation in CAV-1 KO mice

Hematopoietic stem and progenitor cell differentiation in 6- to 8-week-old *CAV-1* KO mice was analyzed by flow cytometry. The differentiation hierarchy was delineated as shown in Figure 1A.[34] c-Kit^{+}Sca-1^{+}Lin$^{neg/low}$ cells, referred to as KSL subset in the literature, contains primitive HSCs and multipotent progenitor cells.[34] As shown in Figure 1B, KSL subsets in WT and *CAV-1* KO mice under normoxia or hypoxia were comparable. However, the HSC pool within the KSL subset was higher in *CAV-1* KO mice under normoxia or hypoxia (Figure 1C). In contrast, the pool of multipotent progenitor cells was lower compared with WT mice independent of hypoxia (Figure 1D-E). Myeloid committed progenitors c-Kit^{+}Sca-1^{-} Lin$^{neg/low}$ (commonly referred to as KL subset) increased in WT mice exposed to hypoxia but were already elevated in *CAV-1* KO mice under normoxic conditions (Figure 1F). Conversely, common myeloid progenitors (CMPs) decreased in WT mice under hypoxia but were already lower in *CAV-1* KO mice under normoxia or hypoxia (Figure 1G). CMPs proliferate and differentiate into granulocyte/monocyte progenitors (GMPs) and megakaryocyte/erythroid progenitors (MEPs).[35] In WT mice, 3 weeks of hypoxia induced an increase in GMP cells. *CAV-1* KO mice exhibited a lower GMP subset (Figure 1H). The MEP subset was higher in *CAV-1* KO mice at baseline levels and remained elevated under hypoxia compared with WT mice (Figure 1I). The data show substantial differences in the frequency myeloid hematopoietic progenitor cell subsets between WT and *CAV-1* KO mice and their response to hypoxia.

Transplantation of CAV-1 KO BM from mice with established PH transfers pulmonary angiogenic and RV remodeling into naive WT mice

BM transplantation was performed to analyze whether BM isolated from mice with established PH can transfer the disease into naive WT mice. PH was induced by exposing naive WT mice and naive *CAV-1* KO to hypoxia (10% O_2) for 3 weeks. Naive animals (WT and *CAV-1* KO) kept under normoxia were used as controls. A schematic representation of the BM transplantation is shown in Figure 2A. Recipients of *CAV-1* KO BM showed increased pulmonary angiogenic remodeling and was the highest in animals receiving hypoxic *CAV-1* KO BM (Figure 2B.) Elevated RVSP was

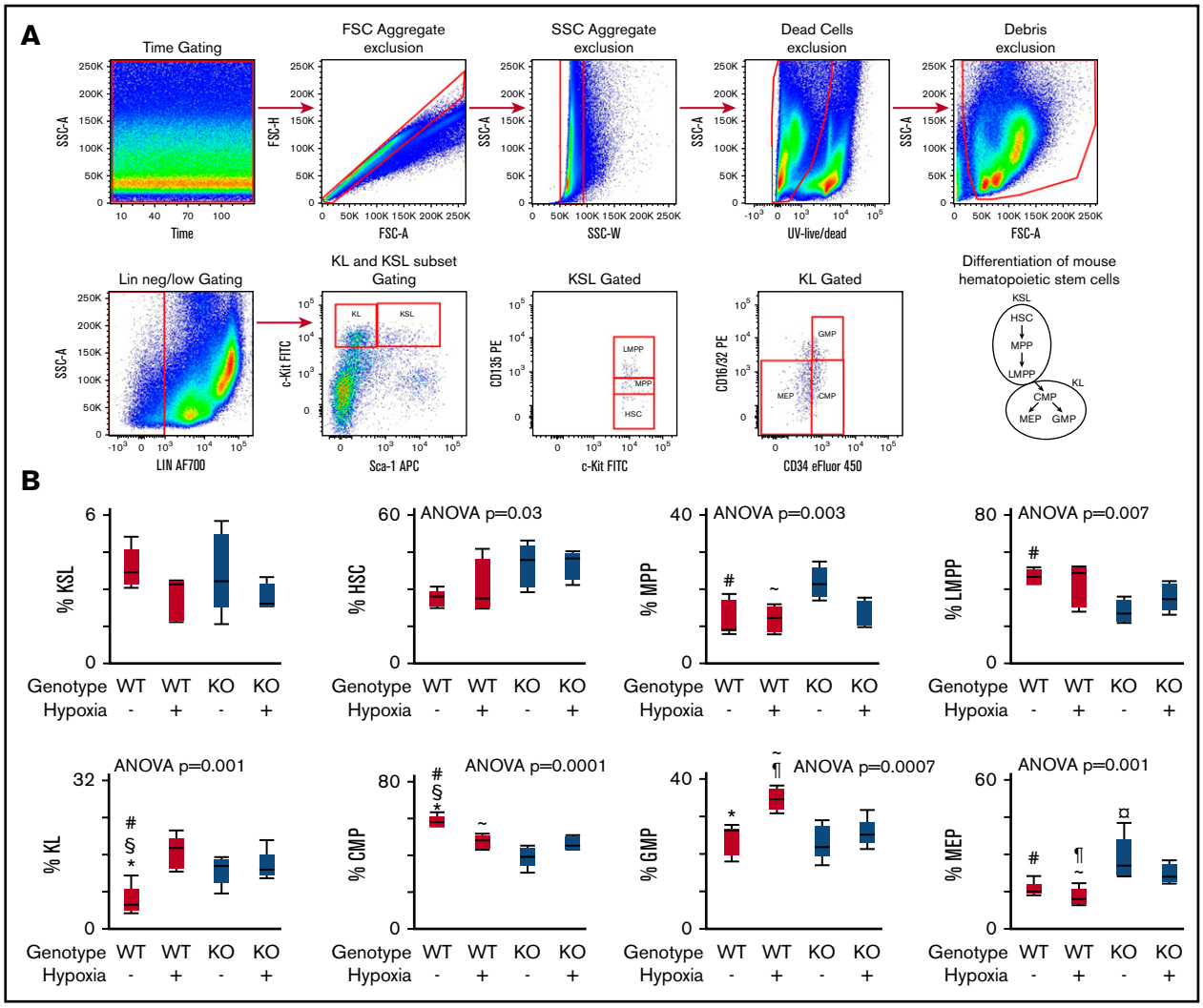

Figure 1. Skewed hematopoietic differentiation in *CAV-1* KO BM. WT or *CAV-1* KO mice under normoxia or 3 weeks of hypoxia were used. BM was isolated from femora and tibiae; mature red blood cells were lysed, and remaining cells were stained for delineation of HSC differentiation using flow cytometry. (A) Gating strategy for HSC and progenitors. Time gating was used to check for and exclude fluidic disturbances in the flow cell. Aggregates were excluded based on blue laser forward and side light scatter (FSC and SSC, respectively) peak height, area, and width. Dead cells were gated out using a UV live/dead stain. Cell debris was eliminated on an FSC/SSC plot. $Lin^{neg/low}$ cells were selected and further gated for primitive and multipotent progenitor cells (KSL) and committed myeloid progenitors (KL) based on standard c-Kit and Sca-1 expression patterns. HSC, MMP, and lymphoid-primed multipotent progenitor (LMPP) subsets were gated in KSL population based on CD135 expression levels. KL population was delineated into CMPs, GMPs, and MEPs based on CD34 and CD16/32 expression. FMO controls were used to set boundaries for stem and progenitor cell gates. A schematic representation of the mouse hematopoietic differentiation path is shown. (B-E) Box plots depicting the percentage of KSL, HSC, MMP, and LMPP subsets in WT and *CAV-1* KO mice, with and without hypoxia exposure. (F-I) Box plots showing the percentage of KL, CMP, GMP, and MEP subsets in WT and *CAV-1* KO mice, with and without hypoxia exposure. Data from 5 male mice in each group are shown. ANOVA values show differences across groups. Symbols represent significant differences between 2 groups ($P < .05$): #WT normoxia vs CAV-1 KO normoxia; ~WT hypoxia vs CAV-1 KO normoxia; §WT normoxia vs CAV-1 KO hypoxia; *WT normoxia vs WT hypoxia; ¶WT hypoxia vs CAV-1 KO hypoxia; ¤CAV-1 KO normoxia vs CAV-1 KO hypoxia. FSC, forward scatter; SSC, side scatter.

observed in recipients of hypoxic *CAV-1* KO, but not in animals transplanted with hypoxic WT or normoxic WT or *CAV-1* KO BM (Figure 2C). RV cardiomyocyte volume was significantly different across groups and the highest in recipients of hypoxic *CAV-1* KO mice (Figure 2D). Future studies of effects on Fulton index (RV mass relative to total heart) may also be assessed in models of PH. RV fibrosis was comparable across groups (Figure 2E). There were no differences in lung arteriole smooth muscle cell hypertrophy in the BM transplantation experiments or *CAV-1* KO mice (data not shown). CAV-1–dependent relaxation of pulmonary smooth muscle cells is impaired in the *CAV-1* KO mice[36] but was not studied in this work. The data demonstrate that BM from *CAV-1* mice with established PH transfers the disease into healthy mice.

Transplantation of naive WT BM into CAV-1 KO mice attenuates development of right heart disease

CAV-1 KO mice spontaneously develop PH during aging. Here, we analyzed whether transplantation of healthy BM into *CAV-1* KO mice before aging-related disease onset could prevent the development of PH. Four-week-old mice underwent BM transplantation and were monitored for 11 months posttransplant (Figure 3A).

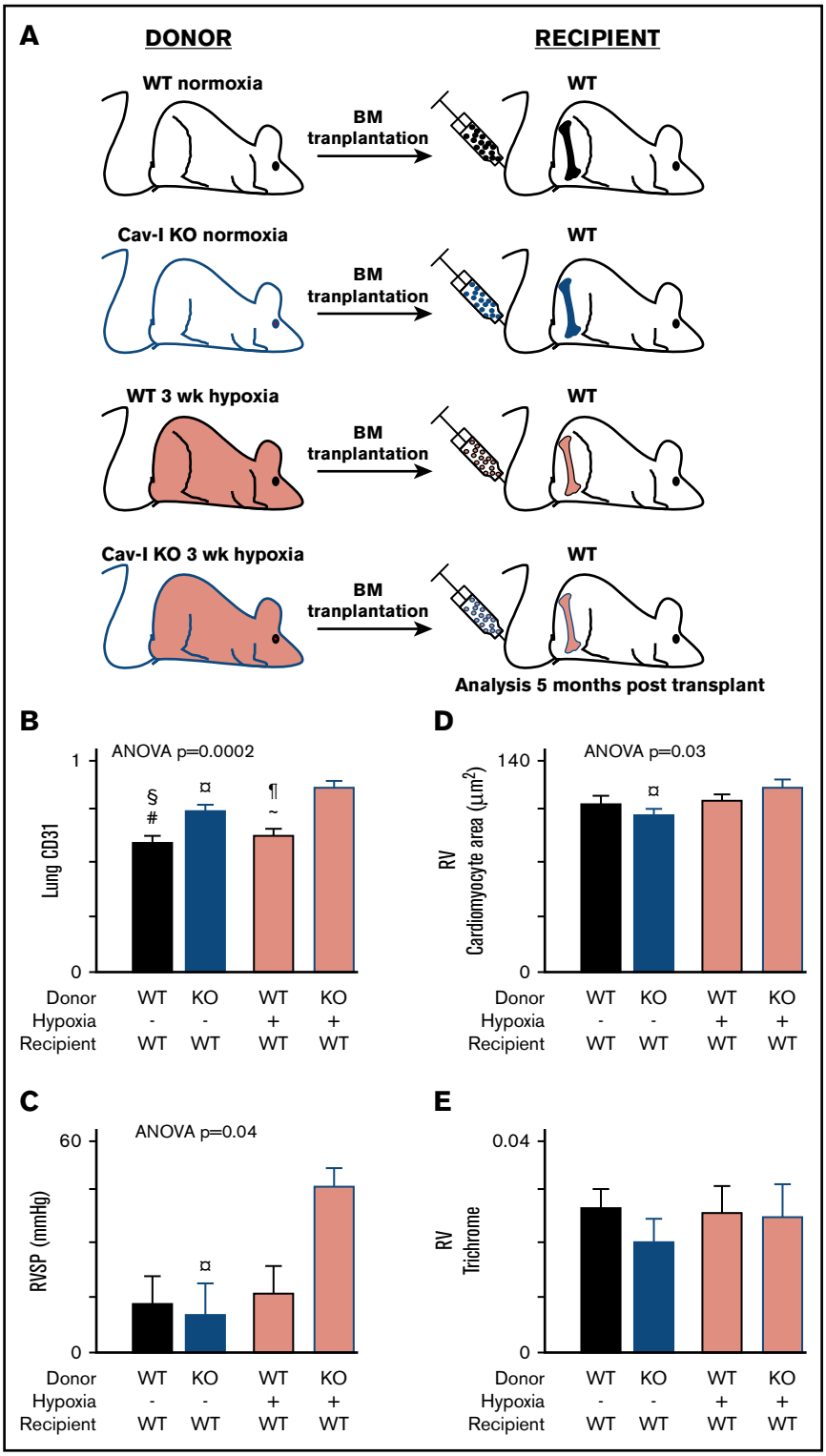

Figure 2. *CAV-1* KO BM from mice with established PH transfers the disease to WT Mice. *CAV-1* KO or WT mice were exposed to hypoxia to induce PH. BM cells were isolated and transplanted in naive WT mice. BM from mice under normoxia used as control transplantation. Recipient mice were analyzed 5 months posttransplant. (A) Schematic representation of the BM transplant experiments. (B) Pulmonary vessel density was measured on lung tissue sections stained for endothelial cell marker CD31. CD31 area/total lung tissue area was quantified and showed that transplantation of *CAV-1* KO BM from mice with established PH (hypoxia) induced endothelial remodeling in the lungs of WT recipient mice. (C) Measurement of RVSP by SPR-1000 Mikro-Tip Catheter into the right ventricle demonstrated that *CAV-1* KO BM engraftment to WT mice led to elevations in RVSP. (D) Quantification of RV cardiomyocyte area to analyze RV hypertrophy. *CAV-1* KO BM from mice with established PH induced hypertrophy of cardiomyocytes in the RV. (E) RV fibrosis was quantified on RV tissue sections stained with trichrome. Trichrome area/total RV area was quantified, and there was no difference across the group, suggesting that the hypertrophy of cardiomyocytes was an adaptive response. Each group contained 4 male mice. Mean ± standard error values are shown. ANOVA values show differences across groups. Symbols represent significant differences between 2 groups ($P < .05$): #WT normoxia vs CAV-1 KO normoxia; ~WT hypoxia vs CAV-1 KO normoxia; §WT normoxia vs CAV-1 KO hypoxia; *WT normoxia vs WT hypoxia; ¶WT hypoxia vs CAV-1 KO hypoxia; ¤CAV-1 KO normoxia vs CAV-1 KO hypoxia.

CAV-1 KO mice transplanted with *CAV-1* KO BM and age- and gender-matched naive WT mice served as controls. Pulmonary angiogenesis remained increased in *CAV-1* KO mice independent of BM genotype (Figure 3B). However, RV hypertrophy and elevation of RVSP were blunted in *CAV-1* KO mice transplanted with WT BM (Figure 3C-D). Moreover, WT BM also prevented the development of RV fibrosis. As anticipated, *CAV-1* KO mice engrafted with *CAV-1* KO BM developed interstitial and perivascular fibrosis, which was inhibited in *CAV-1* KO with reconstituted WT BM (Figure 3E-F). Three female and 2 male mice were used in the BM transplantation experiments. No major gender-specific differences in pulmonary angiogenesis, RV fibrosis, or RVSP (all

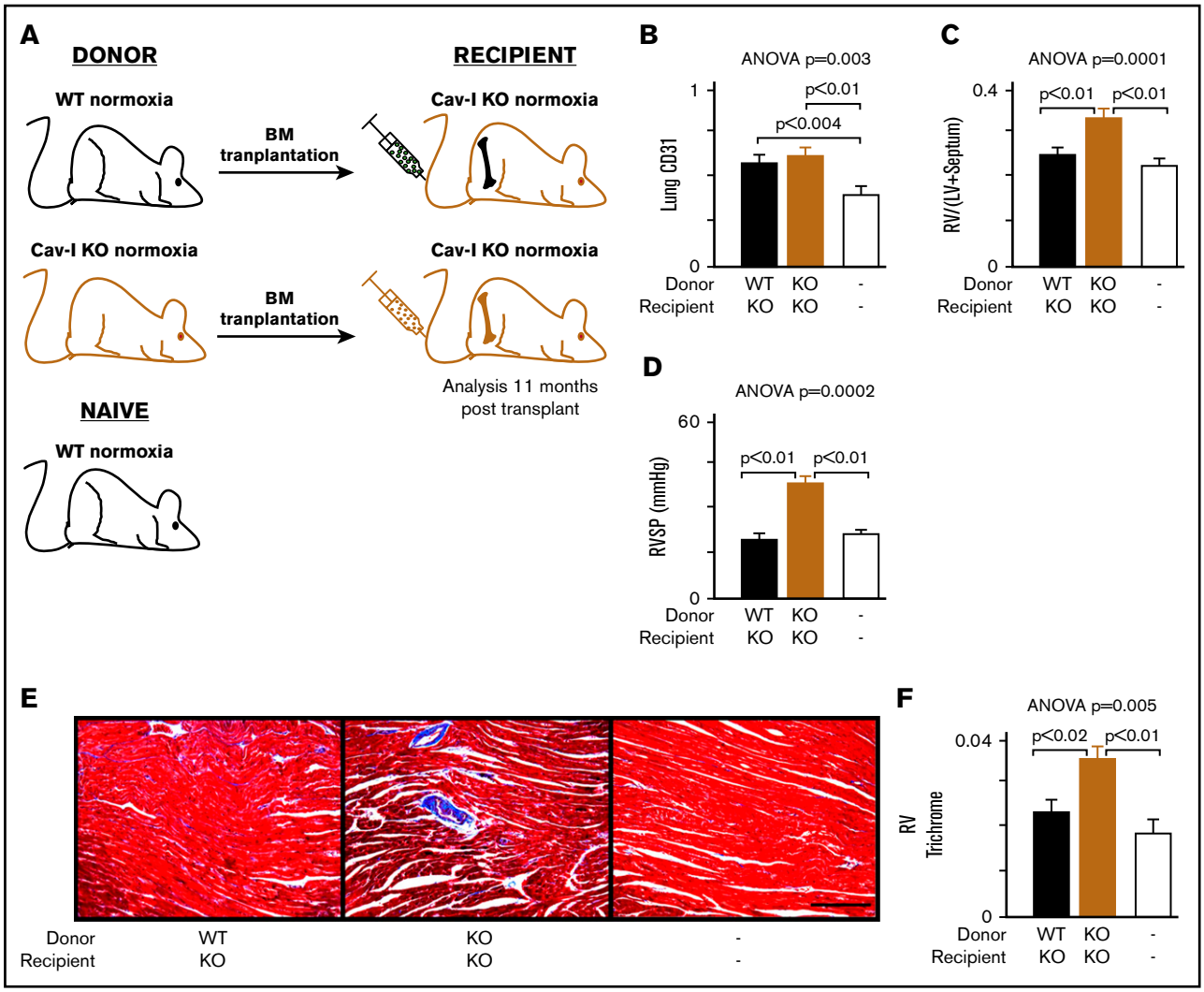

Figure 3. Healthy BM prevents the development of right heart disease in *CAV-1* KO mice. Naive *CAV-1* KO or WT BM was transplanted into naive *CAV-1* KO mice, and mice were monitored for spontaneous development of PH. Naive WT mice were used as an additional control for normal aging. All mice were analyzed 11 months posttransplant. (A) Schematic representation of the experimental setup. (B) Pulmonary vessel density was measured on lung tissue sections stained for the endothelial cell marker CD31. CD31 area/total lung tissue area was quantified, showing that WT BM was not able to inhibit endothelial remodeling in *CAV-1* KO mice. (C) Quantification of RV hypertrophy according to Fulton index [right/(left + septum) ventricular weight] demonstrated that WT BM blocked RV hypertrophy in *CAV-1* KO mice. (D) Measurement of RVSP by SPR-1000 Mikro-Tip Catheter in the RV showed that RVSP was not elevated in *CAV-1* KO mice transplanted with WT BM. (E) RV fibrosis visualized by trichrome staining showed reduced fibrosis in *CAV-1* KO mice transplanted with WT BM. Original magnification ×20. (F) Quantification of the RV fibrosis by measuring trichrome area/total RV area. Each group contained male and female mice (5 mice total in each group). Mean ± standard error are shown. ANOVA values show differences across groups.

$P > .05$) were observed, although the study was not powered to detect this. There were no differences in lung arteriole smooth muscle cell hypertrophy (data not shown). The data demonstrate that transplantation of WT BM into *CAV-1* KO mice could rescue the right ventricle, but not pulmonary endothelial cell proliferation.

Discussion

Accumulating evidence from preclinical models supports that the BM in PH contributes to pulmonary angiogenic remodeling and elevation of RVSP.[23,29,30] Engraftment of serotonin 2B receptor–deficient BM in WT mice protected against the development of hypoxia-induced pulmonary vascular remodeling and elevation of RVSP in mice.[29] In a *Bmpr2* mutant model that spontaneously developed PH without RV remodeling, pulmonary vascular remodeling and elevation of RVSP were shown to be dependent on the BM.[30] Also, xenograft studies with BM isolated from patients showed that PAH BM induced pathological RV hypertrophy.[23] In a prior study, BM from patients with germline *CAV-1* mutation led to a more severe phenotype in the xenografted mice. Here, we used the immunocompetent *CAV-1* KO mouse model to study whether engraftment of healthy BM in *CAV-1* KO mice prevents pulmonary vascular remodeling and development of right heart disease. We first delineated the hematopoietic stem and progenitor cell compartment and found that *CAV-1* KO mice exhibit myeloid abnormalities similar to human PH. Next, we showed that in analogy to human PH BM, *CAV-1* KO BM from mice with hypoxia-induced PH transferred the disease to healthy mice (Figure 4). Intriguingly, engraftment of

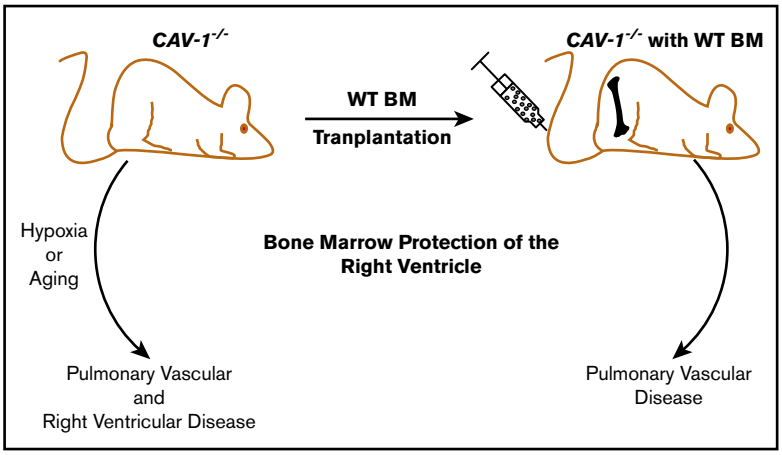

Figure 4. BM in the pathogenesis of PH and RV disease. CAV-1–deficient BM from $CAV^{-/-}$ mice with hypoxia induces pulmonary vascular remodeling and RV hypertrophy. WT BM can protect $CAV^{-/-}$ mice from RV disease that occurs with aging, but not PV disease. Disease-producing BM is skewed to megakaryocyte/erythroid lineage differentiation.

naive WT BM into *CAV-1* KO mice blunted the spontaneous development of RV disease that occurs with aging. The data show that healthy BM protects the right heart from maladaptation independent of pulmonary vascular remodeling.

In xenograft studies using BM from PAH patients, we previously reported that the CMP is skewed toward erythroid-megakaryocyte differentiation.[23] Consistent with this finding, *CAV-1* KO CMP was also skewed toward the erythroid-megakaryocyte lineage independent of hypoxia exposure. Interestingly, while the opposite (increased granulocyte-monocyte differentiation) was observed in WT mice with hypoxia-induced PH, BM from these mice was unable to transfer the disease. Combined with previous studies, the data reveal that while genetically modified BM is able to suppress hypoxia-induced PH,[29] hypoxia-exposed healthy BM is not sufficient to cause PH, suggesting that other pathways in addition to hypoxia are critical in BM-induced PH. The data identify a divergent HSC differentiation pattern of BM that is able and unable to transfer PH. The exact subset of progenitors or mature BM cells that cause the development of PH remains to be elucidated in future studies.

Unexpectedly, engraftment of healthy BM into *CAV-1* KO mice inhibited RV disease, but not pulmonary endothelial cell proliferation, indicating a disconnect between pulmonary vascular remodeling and RV disease. Regardless of severity of pulmonary vasculopathy, the impact of BM on RV changes was striking. Pulmonary vascular remodeling was present in each experimental condition where RV disease was observed, but not vice versa, suggesting that pulmonary vascular remodeling is necessary, but not sufficient, to cause RV disease. During the initial stages of PH, RV hypertrophy induced by elevated RVSP may have a compensatory function. The RV eventually fails when this adaptive RV hypertrophy becomes maladaptive.[37] RV fibrosis, a critical indicator of RV maladaptation, was not observed in our hypoxia studies but was clearly present in the spontaneous development of PH in *CAV-1* KO mice. One potential explanation for this is that animals in the hypoxia studies were not kept long enough to observe the transition from adaptive to maladaptive RV hypertrophy.

Previous elegant work showed that development of pulmonary vascular disease in *CAV-1* KO mice may be due to alternation in endothelial nitric oxide synthase functions.[36] However, expression of endothelial cell–specific CAV-1 in *CAV-1* KO mice inhibited the development of cardiovascular remodeling and pulmonary vascular disease in animals at the ages of 10 or 20 weeks.[38] In contrast, mice were evaluated at the age of 48 weeks in this study. The disparate findings in this paper as compared with prior study may be due to differences in the age of mice used (ie, 48 weeks as compared with 10-20 weeks). Alternatively, it may be that endothelial CAV-1 is required to prevent the pulmonary remodeling and that BM CAV-1 is inadequate. The fact that WT BM rescued the right heart regardless of endothelial CAV-1 deficiency suggests that healthy BM has a critical RV-protective role in conditions of PH.

In summary, the findings here demonstrate that BM from mice with PH can transfer the disease to healthy recipients. Importantly, this work now indicates that healthy BM has a critical RV-protective role independent of pulmonary vascular disease.

Acknowledgments

The authors thank Gerow Joseph and Eric Schultz (Lerner Research Institute [LRI] Flow Cytometry Core) for instrument quality control and setup; Diane Mahovlic, Kelly Simmerman, Eric Diskin, John Peterson, and Judy Drazba (LRI Imaging Core) for assistance with processing and embedding of lung and heart tissues, trichrome staining, quantification of RV fibrosis, and scanning of slides for image quantifications; Amit Vasanji (ImageQ) for assistance with CD31 area quantification; Smarajit Bandyopadhyay (LRI Animal Behavioral Core) for technical assistance with the hypoxia chamber; and Michael Bauer (University of Pittsburgh) for advice and guidance to set up our laboratory for hemodynamic measurements.

This research was funded by National Institutes of Health National Heart, Lung, and Blood Institute grants HL60917 and HL115008 and supported in part by the LRI Center of Excellence in Pulmonary Vascular Disease. S.E. is the Alfred Lerner Chair in Innovative Biomedical Sciences.

Authorship

Contribution: K.A. designed and performed research, analyzed and interpreted data, and wrote the manuscript; N.W., K.W., K.Q., L.G., B.K., and E.S. performed research, analyzed and interpreted the data, and wrote the manuscript; B.G. performed research and wrote the manuscript; and S.E. designed research, analyzed data, and wrote the manuscript.

Conflict-of-interest disclosure: The authors declare no competing financial interests.

Correspondence: Kewal Asosingh, Lerner Research Institute, Cleveland Clinic, Department of Pathobiology, NC22, 9500 Euclid Ave, Cleveland, OH 44195; e-mail: asosink@ccf.org; and Serpil Erzurum, Lerner Research Institute, Cleveland Clinic, Department of Pathobiology, NC22, 9500 Euclid Ave, Cleveland, OH 44195; e-mail: erzurus@ccf.org.

References

1. Rabinovitch M. Molecular pathogenesis of pulmonary arterial hypertension. *J Clin Invest*. 2012;122(12):4306-4313.
2. Rothberg KG, Heuser JE, Donzell WC, Ying YS, Glenney JR, Anderson RG. Caveolin, a protein component of caveolae membrane coats. *Cell*. 1992; 68(4):673-682.
3. Kurzchalia TV, Dupree P, Parton RG, et al. VIP21, a 21-kD membrane protein is an integral component of trans-Golgi-network-derived transport vesicles. *J Cell Biol*. 1992;118(5):1003-1014.
4. Anderson RG. The caveolae membrane system. *Annu Rev Biochem*. 1998;67:199-225.
5. Li S, Couet J, Lisanti MP. Src tyrosine kinases, Galpha subunits, and H-Ras share a common membrane-anchored scaffolding protein, caveolin. Caveolin binding negatively regulates the auto-activation of Src tyrosine kinases. *J Biol Chem*. 1996;271(46):29182-29190.
6. Schlegel A, Pestell RG, Lisanti MP. Caveolins in cholesterol trafficking and signal transduction: implications for human disease. *Front Biosci*. 2000;5: D929-D937.
7. Smart EJ, Ying Y, Donzell WC, Anderson RG. A role for caveolin in transport of cholesterol from endoplasmic reticulum to plasma membrane. *J Biol Chem*. 1996;271(46):29427-29435.
8. Anderson RG, Kamen BA, Rothberg KG, Lacey SW. Potocytosis: sequestration and transport of small molecules by caveolae. *Science*. 1992; 255(5043):410-411.
9. Hulit J, Bash T, Fu M, et al. The cyclin D1 gene is transcriptionally repressed by caveolin-1. *J Biol Chem*. 2000;275(28):21203-21209.
10. Galbiati F, Volonté D, Liu J, et al. Caveolin-1 expression negatively regulates cell cycle progression by inducing G(0)/G(1) arrest via a p53/p21(WAF1/ Cip1)-dependent mechanism. *Mol Biol Cell*. 2001;12(8):2229-2244.
11. Torres VA, Tapia JC, Rodríguez DA, et al. Caveolin-1 controls cell proliferation and cell death by suppressing expression of the inhibitor of apoptosis protein survivin. *J Cell Sci*. 2006;119(Pt 9):1812-1823.
12. Spisni E, Bianco MC, Griffoni C, et al. Mechanosensing role of caveolae and caveolar constituents in human endothelial cells. *J Cell Physiol*. 2003; 197(2):198-204.
13. Scherer PE, Okamoto T, Chun M, Nishimoto I, Lodish HF, Lisanti MP. Identification, sequence, and expression of caveolin-2 defines a caveolin gene family. *Proc Natl Acad Sci USA*. 1996;93(1):131-135.
14. Scherer PE, Lewis RY, Volonte D, et al. Cell-type and tissue-specific expression of caveolin-2. Caveolins 1 and 2 co-localize and form a stable hetero-oligomeric complex in vivo. *J Biol Chem*. 1997;272(46):29337-29346.
15. Bai L, Shi G, Zhang L, et al. Cav-1 deletion impaired hematopoietic stem cell function. *Cell Death Dis*. 2014;5:e1140.
16. Fu Y, Moore XL, Lee MK, et al. Caveolin-1 plays a critical role in the differentiation of monocytes into macrophages. *Arterioscler Thromb Vasc Biol*. 2012; 32(9):e117-e125.
17. Medina FA, Williams TM, Sotgia F, Tanowitz HB, Lisanti MP. A novel role for caveolin-1 in B lymphocyte function and the development of thymus-independent immune responses. *Cell Cycle*. 2006;5(16):1865-1871.
18. Achcar RO, Demura Y, Rai PR, et al. Loss of caveolin and heme oxygenase expression in severe pulmonary hypertension. *Chest*. 2006;129(3): 696-705.
19. Bakhshi FR, Mao M, Shajahan AN, et al. Nitrosation-dependent caveolin 1 phosphorylation, ubiquitination, and degradation and its association with idiopathic pulmonary arterial hypertension. *Pulm Circ*. 2013;3(4):816-830.
20. Duong HT, Comhair SA, Aldred MA, et al. Pulmonary artery endothelium resident endothelial colony-forming cells in pulmonary arterial hypertension. *Pulm Circ*. 2011;1(4):475-486.
21. Nickel NP, Spiekerkoetter E, Gu M, et al. Elafin reverses pulmonary hypertension via caveolin-1-dependent bone morphogenetic protein signaling. *Am J Respir Crit Care Med*. 2015;191(11):1273-1286.
22. Austin ED, Ma L, LeDuc C, et al. Whole exome sequencing to identify a novel gene (caveolin-1) associated with human pulmonary arterial hypertension. *Circ Cardiovasc Genet*. 2012;5(3):336-343.
23. Asosingh K, Farha S, Lichtin A, et al. Pulmonary vascular disease in mice xenografted with human BM progenitors from patients with pulmonary arterial hypertension. *Blood*. 2012;120(6):1218-1227.
24. Mathew R, Huang J, Shah M, Patel K, Gewitz M, Sehgal PB. Disruption of endothelial-cell caveolin-1alpha/raft scaffolding during development of monocrotaline-induced pulmonary hypertension. *Circulation*. 2004;110(11):1499-1506.
25. Jasmin JF, Mercier I, Dupuis J, Tanowitz HB, Lisanti MP. Short-term administration of a cell-permeable caveolin-1 peptide prevents the development of monocrotaline-induced pulmonary hypertension and right ventricular hypertrophy. *Circulation*. 2006;114(9):912-920.
26. Drab M, Verkade P, Elger M, et al. Loss of caveolae, vascular dysfunction, and pulmonary defects in caveolin-1 gene-disrupted mice. *Science*. 2001; 293(5539):2449-2452.

27. Razani B, Engelman JA, Wang XB, et al. Caveolin-1 null mice are viable but show evidence of hyperproliferative and vascular abnormalities. *J Biol Chem*. 2001;276(41):38121-38138.

28. Cruz JA, Bauer EM, Rodriguez AI, et al. Chronic hypoxia induces right heart failure in caveolin-1-/- mice. *Am J Physiol Heart Circ Physiol*. 2012;302(12): H2518-H2527.

29. Launay JM, Hervé P, Callebert J, et al. Serotonin 5-HT2B receptors are required for bone-marrow contribution to pulmonary arterial hypertension. *Blood*. 2012;119(7):1772-1780.

30. Yan L, Chen X, Talati M, et al. Bone marrow-derived cells contribute to the pathogenesis of pulmonary arterial hypertension. *Am J Respir Crit Care Med*. 2016;193(8):898-909.

31. Fulton RM, Hutchinson EC, Jones AM. Ventricular weight in cardiac hypertrophy. *Br Heart J*. 1952;14(3):413-420.

32. Park DS, Cohen AW, Frank PG, et al. Caveolin-1 null (-/-) mice show dramatic reductions in life span. *Biochemistry*. 2003;42(51):15124-15131.

33. Cohen AW, Park DS, Woodman SE, et al. Caveolin-1 null mice develop cardiac hypertrophy with hyperactivation of p42/44 MAP kinase in cardiac fibroblasts. *Am J Physiol Cell Physiol*. 2003;284(2):C457-C474.

34. Mayle A, Luo M, Jeong M, Goodell MA. Flow cytometry analysis of murine hematopoietic stem cells. *Cytometry A*. 2013;83(1):27-37.

35. Orkin SH, Zon LI. Hematopoiesis: an evolving paradigm for stem cell biology. *Cell*. 2008;132(4):631-644.

36. Zhao YY, Zhao YD, Mirza MK, et al. Persistent eNOS activation secondary to caveolin-1 deficiency induces pulmonary hypertension in mice and humans through PKG nitration. *J Clin Invest*. 2009;119(7):2009-2018.

37. Ryan JJ, Archer SL. The right ventricle in pulmonary arterial hypertension: disorders of metabolism, angiogenesis and adrenergic signaling in right ventricular failure. *Circ Res*. 2014;115(1):176-188.

38. Murata T, Lin MI, Huang Y, et al. Reexpression of caveolin-1 in endothelium rescues the vascular, cardiac, and pulmonary defects in global caveolin-1 knockout mice. *J Exp Med*. 2007;204(10):2373-2382.